Properties of the primary somatosensory cortex projection to the primary motor cortex in the mouse

Iraklis Petrof, Angela N. Viaene and S. Murray Sherman

J Neurophysiol 113:2400-2407, 2015. First published 28 January 2015; doi:10.1152/jn.00949.2014

Journal of Neurophysiology publishes original articles on the function of the nervous system. It is published 12 times a year (monthly) by the American Physiological Society, 9650 Rockville Pike, Bethesda MD 20814-3991. ISSN: 0022-3077, ESSN: 1522-1598. Visit our website at http://www.the-aps.org/.

J Neurophysiol 113: 2400–2407, 2015.
First published January 28, 2015; doi:10.1152/jn.00949.2014.

Properties of the primary somatosensory cortex projection to the primary motor cortex in the mouse

Iraklis Petrof, Angela N. Viaene, and S. Murray Sherman
Department of Neurobiology, University of Chicago, Chicago, Illinois

Submitted 25 November 2014; accepted in final form 22 January 2015

Petrof I, Viaene AN, Sherman SM. Properties of the primary somatosensory cortex projection to the primary motor cortex in the mouse. *J Neurophysiol* 113: 2400–2407, 2015. First published January 28 2015; doi:10.1152/jn.00949.2014.—The primary somatosensory (S1) and primary motor (M1) cortices are reciprocally connected, and their interaction has long been hypothesized to contribute to coordinated motor output. Very little is known, however, about the nature and synaptic properties of the S1 input to M1. Here we wanted to take advantage of a previously developed sensorimotor slice preparation that preserves much of the S1-to-M1 connectivity (Rocco MM, Brumberg JC. *J Neurosci Methods* 162: 139–147, 2007), as well as available optogenetic methodologies, in order to investigate the synaptic profile of this projection. Our data show that S1 input to pyramidal cells of M1 is highly homogeneous, possesses many features of a "driver" pathway, such as paired-pulse depression and lack of metabotropic glutamate receptor activation, and is mediated through axons that terminate in both small and large synaptic boutons. Our data suggest that S1 provides M1 with afferents that possess synaptic and anatomical characteristics ideal for the delivery of strong inputs that can "drive" postsynaptic M1 cells, thereby potentially affecting their output.

barrel cortex; corticocortical pathway; drivers; motor cortex; sensorimotor integration

THE MOTOR CORTEX (M1) is the portion of cortex that provides the spinal cord with input that determines much of an organism's motor actions. M1 receives direct and indirect inputs from multiple cortical and thalamic areas, including premotor, executive, and sensory centers (Asanuma and Hunsperger 1975; Cicirata et al. 1986; Horne and Tracey 1979; Muakkassa and Strick 1979; Porter and White 1983; Reep et al. 1990), and, as a result, its output is thought to be determined by both internally driven and sensory-driven factors. Input from the primary somatosensory cortex (S1) to M1 has long been speculated to contribute to sensorimotor integration and to be a major determinant of M1's output. This is supported by the observation that discontinuation of S1 input to M1 can disrupt many motor behaviors in primates and felines (Brochier et al. 1999; Hiraba et al. 2000; Lin et al. 1993; Pavlides et al. 1993).

A common problem with the electrophysiological study of long-distance, interareal corticocortical pathways is the difficulty of preserving them in slice preparations, which often limits their study to the description of their anatomical features. However, understanding the function of such corticocortical pathways, like the one from S1 to M1, and their functional role within cortical networks requires among others a detailed study of their physiological and synaptic characteristics, much of which can be achieved in vitro. Recent advances in the development of viable slice preparations and the emergence of optogenetics have created fertile ground for the better delineation and understanding of previously difficult-to-study pathways.

Using a sensorimotor slice preparation that preserves much of the S1-to-M1 connectivity, previous in vitro studies have reported that S1 input to M1 is monosynaptic and that it produces large postsynaptic responses, particularly in infragranular layers of M1 (Rocco and Brumberg 2007; Rocco-Donovan et al. 2011). We wanted to take advantage of this slice preparation, as well as available optogenetic methodologies, to further investigate the synaptic profile of this projection. Studies of glutamatergic inputs between cortex and thalamus (Li et al. 2003; Petrof and Sherman 2009; Reichova and Sherman 2004; Viaene et al. 2011a, 2011b, 2011c), but also within sensory areas of the cortex (Covic and Sherman 2011; DePasquale and Sherman 2011), have shown that most of these inputs can be classified on the basis of their synaptic and anatomical characteristics into Class 1 or Class 2 types (see Sherman 2012). We have previously argued that those classified as Class 1 inputs, by virtue of their synaptic properties, are better equipped to exert strong postsynaptic effects on their targets and thus are likely to be main information carriers. Class 1 inputs have been further subdivided into Classes 1A, 1B, and 1C on the basis of the degree and nature of their convergence on postsynaptic cells and the probability of transmitter release from synaptic terminals (Viaene et al. 2011c; reviewed in Sherman and Guillery 2013). On the other hand, the postsynaptic effects of Class 2 inputs are generally weaker, slower, and longer-lasting, making them less ideal for information transfer and better suited for the modulation of ongoing cellular activity. Here we show that the S1 input to M1 possesses Class 1 characteristics that may allow it to exert strong postsynaptic effects that can "drive" M1 cells and therefore strongly affect their output.

METHODS

Animals. BALB/c mice of both sexes and of ages noted below were used for these experiments.

Slice preparation. Slices containing connectivity between the primary sensory and motor areas of cortex (S1 and M1, respectively) were prepared from mice aged 21–60 days old as previously described by Rocco and Brumberg (2007). Briefly, animals were deeply anesthetized with isoflurane and were then decapitated. Brains were removed and placed in cold (0–4°C), oxygenated (95% O_2-5% CO_2) slicing solution containing (in mmol) 2.5 KCl, 1.25 NaH_2PO_4, 10 $MgCl_2$, 0.5 $CaCl_2$, 26 $NaHCO_3$, 11 glucose, and 206 sucrose. Sensorimotor slices (450 μm thick) were cut parasagittally as follows: Brains were hemisected, and the medial surface was glued onto a

Address for reprint requests and other correspondence: S. M. Sherman, Dept. of Neurobiology, Univ. of Chicago, 947 E. 58th St., MC 0926, 316 Abbott, Chicago, IL 60637 (e-mail: msherman@bsd.uchicago.edu).

45°-angled block of agar with the rostral end pointing upward. Slices were cut with a vibratome (Leica, Wetzlar, Germany) and were kept in artificial cerebrospinal fluid containing (in mmol) 125 NaCl, 3 KCl, 1.25 NaH_2PO_4, 1 $MgCl_2$, 2 $CaCl_2$, 25 $NaHCO_3$, and 25 glucose, at room temperature. All procedures were carried out in accordance with protocols reviewed and approved by the Institutional Animal Care and Use Committee of the University of Chicago.

Adeno-associated virus injections. For optogenetic experiments, seven mice (aged 21–55 days) were anesthetized with a mixture of ketamine (100 mg/kg) and xylazine (3 mg/kg) and stereotaxically injected with AAV5-CaMKIIa-hChR2(H134R)-EYFP (University of North Carolina VectorCore, with permission from K. Deisseroth) in S1. We chose this particular promoter and serotype to ensure that only cell bodies of excitatory cells would take up the virus and transport it anterogradely (Tye et al. 2011). Coordinates were determined by the Franklin and Paxinos (2008) mouse brain atlas (distances are mm from bregma): AP: −0.9, ML: −3.0, DV: −1.5. Animals were allowed to recover for at least 14 days before electrophysiology experiments could commence. After inspection of the injections, three animals were not considered further, given that the injections were either nonspecific to S1 or resulted in channelrhodopsin 2 expression that was too weak. The optogenetic data presented here came from the remaining four animals. Sensorimotor slices from these four animals were prepared as described above.

Electrophysiology. Whole cell recordings were performed in a visualized slice setup under a differential interference contrast (DIC)-equipped microscope to image thalamic and cortical structures. Current- and voltage-clamp signals were collected and amplified with pCLAMP software and a Multiclamp 700B amplifier (Axon Instruments). All data were digitized on a Digidata 1200 board (Axon Instruments) and analyzed in Clampfit (Axon Instruments) software.

Recording glass pipettes (input resistances 3–7 MΩ) were filled with intracellular solution containing (in mmol) 117 K-gluconate, 13 KCl, 1 $MgCl_2$, 0.07 $CaCl_2$, 10 HEPES, 0.1 EGTA, 2 Na_2-ATP, 0.4 Na-GTP, and 0.003 chloride channel blocker TS-TM calix[4]arene (generously provided by R. J. Bridges, Rosalind Franklin University, Chicago, IL), with 0.02% biocytin, pH 7.3, 290 mosM.

Individual cortical areas and layers were identified under DIC, using established landmarks and cytoarchitectonic criteria (such as the relative density of cells), respectively. S1 was identified by the presence of barrel fields, and its layers were distinguished on the basis of their cellular density. In our slice preparation, M1 could be identified as the area immediately lateral (~500 μm) to the most medial aspect of cortex (i.e., the longitudinal fissure), an area that we had previously routinely seen labeled anterogradely after biotinylated dextran amine (BDA) injections in S1 (see below). M1 layers were identified on the basis of their relative depth from cortical surface, using previously published information (Hooks et al. 2011; Mao et al. 2011). When patching a cell, transition zones between cortical areas or between layers were avoided to minimize the risk of misidentifying layers or areas sampled. Electrical stimulation was delivered by a concentric bipolar electrode (FHC) at locations indicated by glutamate photo-uncaging (see below).

The assessment of short-term plasticity (depression vs. facilitation) was carried out by using a stimulation protocol consisting of four 0.1-ms-long, positive current pulses at a frequency of 10 Hz. Initially this was done only for the lowest stimulation intensity capable of consistently inducing excitatory postsynaptic potentials (EPSPs) larger than 0.5 mV in the recorded cells. Subsequently, however, we also examined the effects of increased stimulation currents on evoked responses (see RESULTS).

To induce and isolate metabotropic glutamate receptor activation, we used a high-frequency stimulation protocol (0.1-ms-long pulses delivered at 125 Hz over 200–800 ms, 100–300 μA) combined with the application of NMDA and AMPA receptor antagonists (100 μM AP5 and 50 μM DNQX, respectively).

The latency of an EPSP was measured as the time between stimulation onset and the initiation of the evoked EPSP. We used criteria described previously (Viaene et al. 2011a) to assess the monosynaptic nature of the recorded responses. An EPSP2-to-EPSP1 ratio (E2/E1) was calculated by dividing the amplitude of the second EPSP by the amplitude of the first EPSP. An E2/E1 > 1 indicates paired-pulse facilitation, whereas an E2/E1 < 1 indicates paired-pulse depression.

Glutamate uncaging and optical stimulation. For photo-uncaging of glutamate, nitroindolinyl-caged glutamate (Sigma-Aldrich, St. Louis, MO) was added to the recirculating artificial cerebrospinal fluid (0.4 mM) and a laser beam (DPSS Laser, Santa Clara, CA) was used to locally photolyse the caged compound. The laser beam had an intensity of 20–80 mW, and laser illumination lasted 2 ms (450- to 490-nm wavelength, frequency-tripled Nd: YVO4, 100-kHz pulse repetition rate). Custom-made software written in MATLAB (MathWorks) was used to control the laser. The same laser was also used to optically stimulate the S1-originating terminals in M1 in slices obtained from animals that had been injected with adeno-associated virus (AAV).

BDA injections and immunohistochemistry. For neuroanatomical tracing experiments, we used the same coordinates as above to iontophoretically inject 5% BDA (10,000 mol wt, Molecular Probes) in S1 of three animals. After a 72-h recovery period, the animals were deeply anesthetized with ketamine-xylazine and transcardially perfused with phosphate-buffered saline (PBS) followed by 4% paraformaldehyde in PBS. Brains were saturated overnight in 10–30% sucrose in paraformaldehyde, and 35-μm-thick coronal sections were cut with a sliding microtome. Slices were processed for BDA as described previously (Viaene et al. 2011b). After processing, sections were mounted onto gelatinized slides, dehydrated, and coverslipped.

Brain sections were examined under a microscope (Leica Microsystems) and photos of terminal fields in all layers of M1 taken at ×100 with a Retiga2000 monochrome CCD camera and QCapture Pro software (QImaging). The resolution of the digital images used for the bouton area measurements was 1,600 × 1,200 pixels, and the size of each pixel was 7.5 μm. The plane of focus was determined by the person taking the photographs.

RESULTS

Glutamate uncaging hotspots. After patching a cell in M1, photo-uncaging of glutamate was used to reveal the locations within S1 that contained cells projecting to the patched cell (we called these locations "hotspots"; Fig. 1*A*). In our slice, hotspots were always found within layer 5 of S1 and occasionally were big enough to extend into layer 6. A concentric bipolar electrode was placed within the identified hotspot in order to electrically stimulate the S1 cells projecting to the patched cell in M1. We used the "hotspot" approach for all M1 cells that were tested with electrical stimulation, with the exception of those cells that were collected from animals previously injected with AAV (see below).

Responses to electrical stimulation. In total we recorded from 42 regular-spiking pyramidal cells in M1. Stimulation of S1 produced monosynaptic responses in 24 cells (11 in layers 2/3, 10 in layer 5, and 3 in layer 6 of M1). The remaining 18 cells did not produce any responses after stimulation of S1 inputs and were not considered further. Responsive cells in layers 2/3 of M1 had a membrane potential of −58.83 ± 8.2 (SD) mV, uncorrected for an approximately −10-mV junction potential, and an input resistance of 452.3 ± 69.1 MΩ. Responsive cells in layer 5 had an uncorrected membrane potential of −57.7 ± 7.9 mV and an input resistance of 426.1 ±

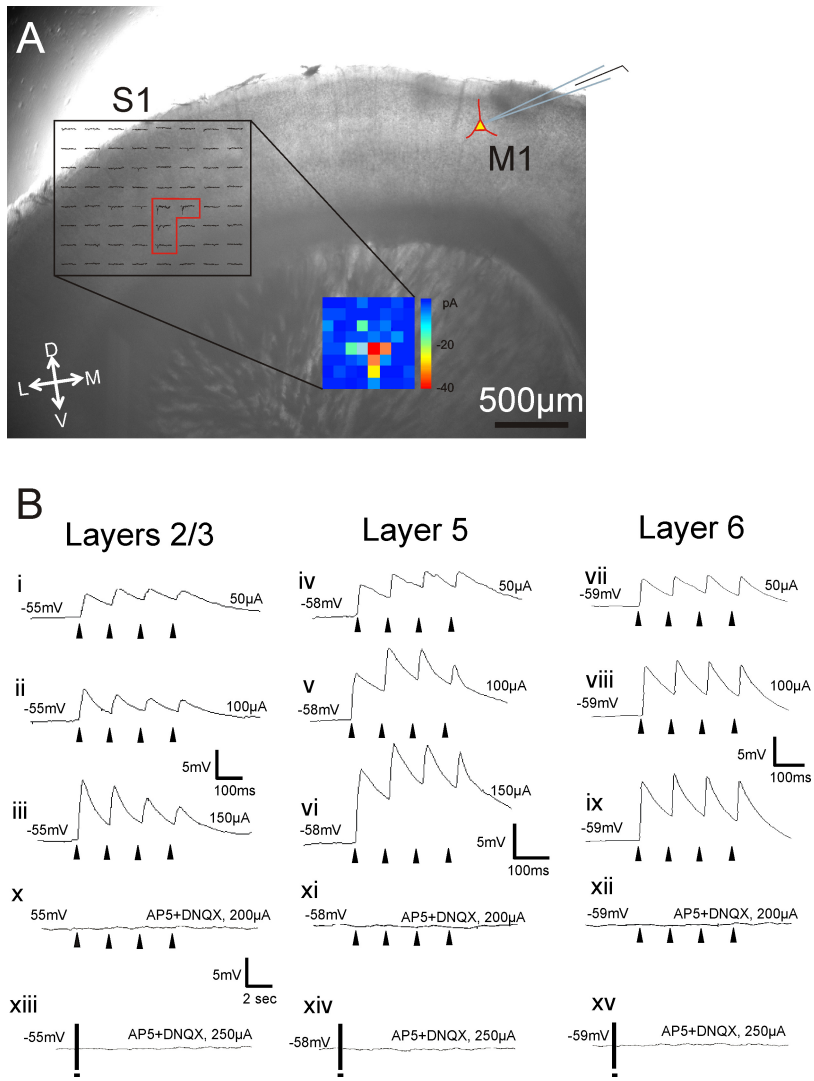

Fig. 1. Responses of primary motor cortex (M1) cells during primary somatosensory cortex (S1) stimulation. *A*: glutamate photo-uncaging over an area of S1 (black square) reveals hotspot of inputs into patched M1 cell. Red outline indicates the hotspot. *Inset*: false-color map of location and magnitude of inward currents. Each pixel corresponds to a locus of uncaging as seen in the main figure. D, dorsal; L, lateral; M, medial; V, ventral. *B*: responses of M1 cells in layers 2/3, 5, and 6 to 10-Hz electrical stimulation applied within identified S1 hotspots at increasing stimulation intensities (*i–ix*). Excitatory postsynaptic potentials (EPSPs) could be completely blocked by the AMPA and NMDA receptor antagonists AP5 and DNQX (*x–xii*). High-frequency electrical stimulation (125 Hz) in the presence of AP5 and DNQX did not produce a change in membrane potential, reflecting the lack of a metabotropic glutamate receptor activation in this pathway (*xiii–xv*).

69.72 MΩ, while those in layer 6 had an uncorrected membrane potential of −56.61 ± 10.9 mV and an input resistance of 417.4 ± 86.82 MΩ.

Every responsive cell that we recorded from in M1, regardless of layer, responded to electrical stimulation of its identified S1 hotspot with what we have previously called a "Class 1B" response pattern (Covic and Sherman 2011; DePasquale and Sherman 2011; Viaene et al. 2011c). (A difference between Class 1A, first defined with respect to inputs to thalamic relay cells, and Class 1B is that the latter shows evidence of more convergence of inputs; reviewed in Sherman and Guillery 2013). More specifically, cells responded with paired-pulse depression, meaning that during a brief 10-Hz stimulation the amplitude of the second evoked EPSP was smaller than that of the first EPSP. The paired-pulse depression pattern was maintained regardless of the stimulation intensity used. (see Fig. 1*B*, *i–ix*). All responses could be entirely eliminated by AP5 and DNQX (Fig. 1*B*, *x–xii*). High-frequency stimulation (125 Hz) in the presence of NMDA and AMPA antagonists did not produce any responses (Fig. 1*B*, *xiii–xv*), suggesting a lack of metabotropic glutamate receptor activation in this pathway.

Cells in all layers of M1 produced EPSP amplitudes that showed a monotonic relationship with stimulation intensity (see Fig. 2*A*), a very common feature in corticocortical pathways (Covic and Sherman 2011; DePasquale and Sherman 2011). The amplitude of the first EPSP of each response was larger for layer 5 cells than cells in layers 2/3 and 6 (Mann-Whitney, $P < 0.05$; Fig. 2*B*). An inspection of the E2/E1 ratio revealed that cells in layer 5 of M1 depressed more (E2/E1 = 0.69) than those in layers 2/3 (E2/E1 = 0.8, Mann-Whitney, $P = 0.023$) and layer 6 (E2/E1 = 0.85, Mann-Whitney, $P = 0.015$; see Fig. 2*C*). Finally, response latencies in layer 2/3 cells were significantly longer than those in layers 5 and 6 (Mann-Whitney, $P < 0.05$; Fig. 2*D*).

Responses to optical stimulation. A noteworthy disadvantage of electrical stimulation is that it can activate not only cell bodies but also axons of passage. As mentioned above, we tried to minimize the effect of potential axonal stimulation by using caged glutamate photostimulation to identify input "hotspots" within S1. Nonetheless, we wanted to see whether the synaptic profile of the S1-to-M1 input we observed with electrical stimulation would be the same if we stimulated the pathway optically, thus eliminating entirely the possibility of axon-of-passage stimulation.

For that purpose, we patched M1 cells in animals that had been previously injected with AAV5-CaMKIIa-

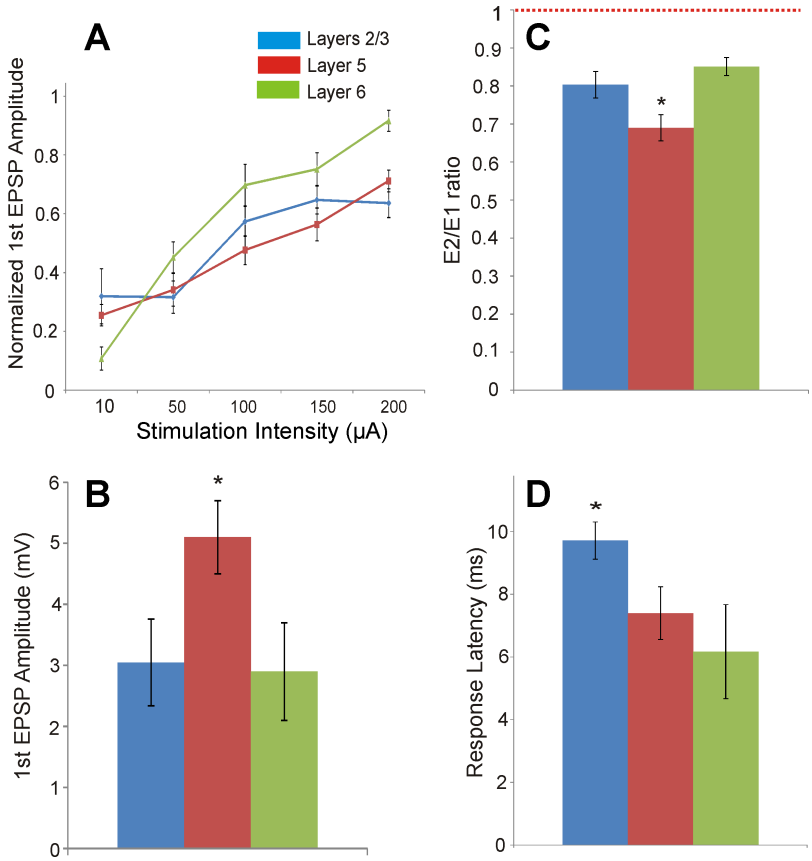

Fig. 2. Response properties of M1 cells during S1 electrical stimulation, broken down by layer. *A*: normalized 1st EPSP amplitudes for cells in layers 2/3, 5, and 6 of M1, across different S1 stimulation intensities. Gradual increases in stimulation intensity resulted in gradual EPSP amplitude increases in all layers. Data were normalized using the value of the greatest response amplitude produced by each cell for each particular stimulation intensity. *B*: average 1st EPSP amplitude during minimal stimulation intensity (typically ~10 μA) in M1 cells of layers 2/3, 5, and 6. *C*: average EPSP2-to-EPSP1 ratio (E2/E1) of M1 cells in layers 2/3, 5, and 6. *D*: average response latency times for cells in layers 2/3, 5, and 6 in M1. $^*P < 0.05$.

hChR2(H134R)-EYFP in S1 (Fig. 3*A*). The injections resulted in widespread expression of channelrhodopsin throughout all layers of S1 (successful injections were centered near the border between layers 4 and 5). Furthermore, channelrhodopsin-positive axons and terminals originating in S1 could be seen throughout M1, but particularly in layers 2/3 and layer 5 (Fig. 3*B*). We patched cells in layers 2/3, 5, and 6 of M1 and stimulated them directly with a laser. All three cells we patched in layers 2/3 and three of five cells in layer 5 of M1 responded to stimulation with excitatory postsynaptic currents (EPSCs). Of the four cells patched in layer 6 of M1, only one responded to laser stimulation. When stimulated with a 10-Hz laser pulse, all responsive cells in M1 produced EPSCs showing paired-pulse depression (Fig. 3*C*, *bottom*). We also wanted to see how these particular cells would respond to electrical stimulation of S1. Laser photo-uncaging of glutamate for the identification of input hotspots could not be used in slices expressing channelrhodopsin because of the potential simultaneous activation of both channelrhodopsin and the caged glutamate. Instead, we placed an electrical stimulator in layer 5 of S1 and carefully moved it around within S1 until a monosynaptic response was seen in the recorded M1 cell. We did so while using minimal stimulation intensity (lowest stimulation intensity capable of consistently inducing EPSPs larger than 0.5 mV in the recorded cells). Every responsive M1 cell that we tested with optical stimulation responded to 10-Hz electrical stimulation with paired-pulse depression (Fig. 3*C*, *top*), and the average E2/E1 was 0.71 ($\pm$0.27). None of the M1 cells that failed to respond to optogenetic stimulation responded to electrical stimulation.

Bouton sizes. BDA injections in S1 produced extensive anterograde labeling within M1, with most of the labeling seen in layers 2/3 and upper layer 5 and with considerably less labeling seen in lower layer 5 and layer 6 (Fig. 4). Because of the very small number of boutons in layer 6 we decided to focus on layers 2/3 and 5, and we measured 500 boutons in each of these layers. The average size of boutons in layers 2/3 (0.81 ± 0.39 μm^2) was not significantly different from those in layer 5 (0.84 ± 0.51 μm^2, Mann-Whitney, $P > 0.05$). Bouton size data from layers 2/3 and 5 were pooled together and plotted against bouton sizes from two pathways that have been respectively classified as Class 1 and Class 2 (Viaene et al. 2011b), namely, the pathway from the ventral division of the medial geniculate nucleus to layer 4 of the primary auditory cortex (Class 1A) and the pathway from the ventral division of the medial geniculate body to layers 2/3 of the auditory cortex (mostly Class 2) (Fig. 4*E*). Whereas overall bouton sizes of the S1-to-M1 pathway were different from those of both above-mentioned pathways (2-sample Kolmogorov-Smirnov test, $P < 0.01$), its distribution includes a substantial tail of larger boutons (>1.2 μm^2), which is typical of other Class 1 pathways we have measured (Covic and Sherman 2011; Viaene et al. 2011a, 2011b, 2011c).

DISCUSSION

Using a slice preparation that contained connectivity between S1 and M1, we found that stimulation of S1 produced very similar responses across all layers of M1 from which we could obtain monosynaptic responses. These responses exhibited synaptic paired-pulse depression (after both electrical and

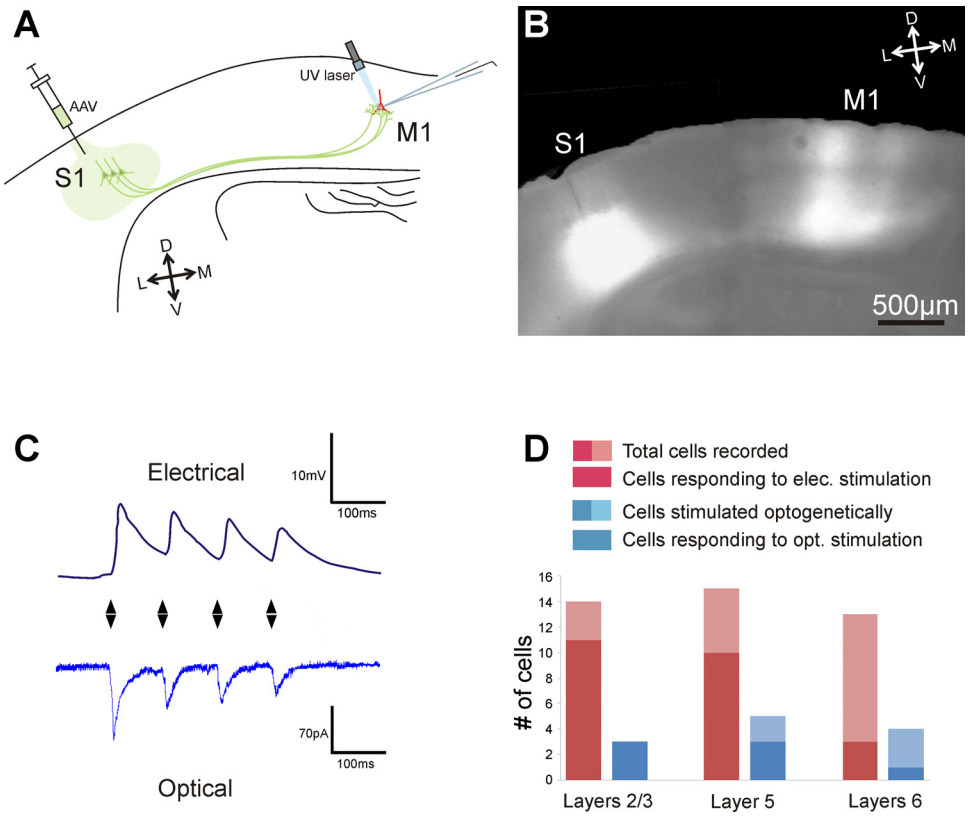

Fig. 3. Optogenetic stimulation of the S1-to-M1 pathway. *A*: diagrammatic representation of the methods used. Adeno-associated virus (AAV) was injected in the S1 of animals in vivo. Infected S1 cells expressed channelrhodopsin on their somata, axons, and terminals. Subsequently, we recorded from M1 cells and used a laser beam to activate channelrhodopsin-expressing terminals originating in S1. *B*: example of an AAV injection site in S1 as seen under fluorescent light. Fluorescence indicates the expression of channelrhodopsin. Channelrhodopsin expression can also be seen along axons traveling to M1, and within M1 itself. *C*, *bottom*: typical responses of M1 cells to optogenetic stimulation. *Top*: responses of the same cell to electrical stimulation of S1. *D*: summary of the recorded cells for each layer of M1. Red/pink bars represent the total number of cells recorded and stimulated electrically (included are those cells that were stimulated both optically and electrically). The red portion of the bars represents the number of cells that responded to electrical stimulation, while pink represents cells that did not respond to electrical stimulation. Blue/cyan bars represent the number of cells that were stimulated optogenetically. The blue portion of the bars represents the cells that responded to optogenetic stimulation, while cyan represents unresponsive cells. Cells that responded to optogenetic stimulation always responded to electrical stimulation too. Cells that did not respond to optogenetic stimulation did not respond to electrical stimulation either.

optical stimulation) and a graded activation profile and showed no evidence of metabotropic glutamate receptor activation. These synaptic characteristics let us classify the S1-to-M1 inputs as Class 1 (and more specifically as Class 1B, see below). Furthermore, our anatomical data supported this classification, since the S1-to-M1 pathway terminates in both small and large boutons, a feature that is seen in all Class 1 inputs but never in Class 2 inputs, which are associated with small boutons only.

Our sample of recorded cells does not include layer 4, which we were unable to identify in our slices. There is some evidence that layer 4 exists in motor cortex of rats (Skoglund et al. 1997), monkeys (Garcia-Cabezas and Barbas 2014), ferrets (Rowell et al. 2010), and mice (Yamawaki et al. 2014), and so it is possible that some of our recorded cells identified as in layers 2/3 or 5 could have been in layer 4.

The synaptic features of the S1-to-M1 pathway described here are characteristic of what we have previously referred to as a subset of Class 1 inputs, namely "Class 1B" (Covic and Sherman 2011; DePasquale and Sherman 2011; Viaene et al. 2011c). In the context of sensory information transfer, Class 1 inputs have been hypothesized to constitute main information-bearing pathways that determine receptive field properties of postsynaptic neurons (Sherman and Guillery 2013). Class 1 inputs have been subdivided into Class 1A, B, and C inputs, on the basis of minor differentiating features (see Viaene et al. 2011b), but they are all thought to represent pathways relaying information that can "drive" postsynaptic cells. For this reason Class 1 pathways have previously been referred to as "drivers," especially when describing them in thalamus (Reichova and Sherman 2004; Sherman and Guillery 2013). In contrast, Class 2 inputs (formerly referred to also as "modulators"), which are characterized by paired-pulse facilitation and the activation of both ionotropic and metabotropic glutamate receptors, are thought to be responsible for influencing (modulating) the way information is transmitted (DePasquale and Sherman 2012, 2013; Lam and Sherman 2013; Lee and Sherman 2009; Liu et al. 2014; Reichova and Sherman 2004; Sherman and Guillery 2013; Viaene et al. 2011a). We saw no evidence of Class 2 inputs in M1 during either electrical or optical stimulation of S1.

The graded pattern of response amplitudes we saw in M1 cells after electrical stimulation of S1 is an indication that many axons originating in S1 converge onto individual M1 cells. Increasing stimulation intensities in S1 result in the recruitment of a progressively larger number of afferent axons, and thus (when these axons terminate on the same M1 cell) in progressively larger postsynaptic responses. This feature dis-

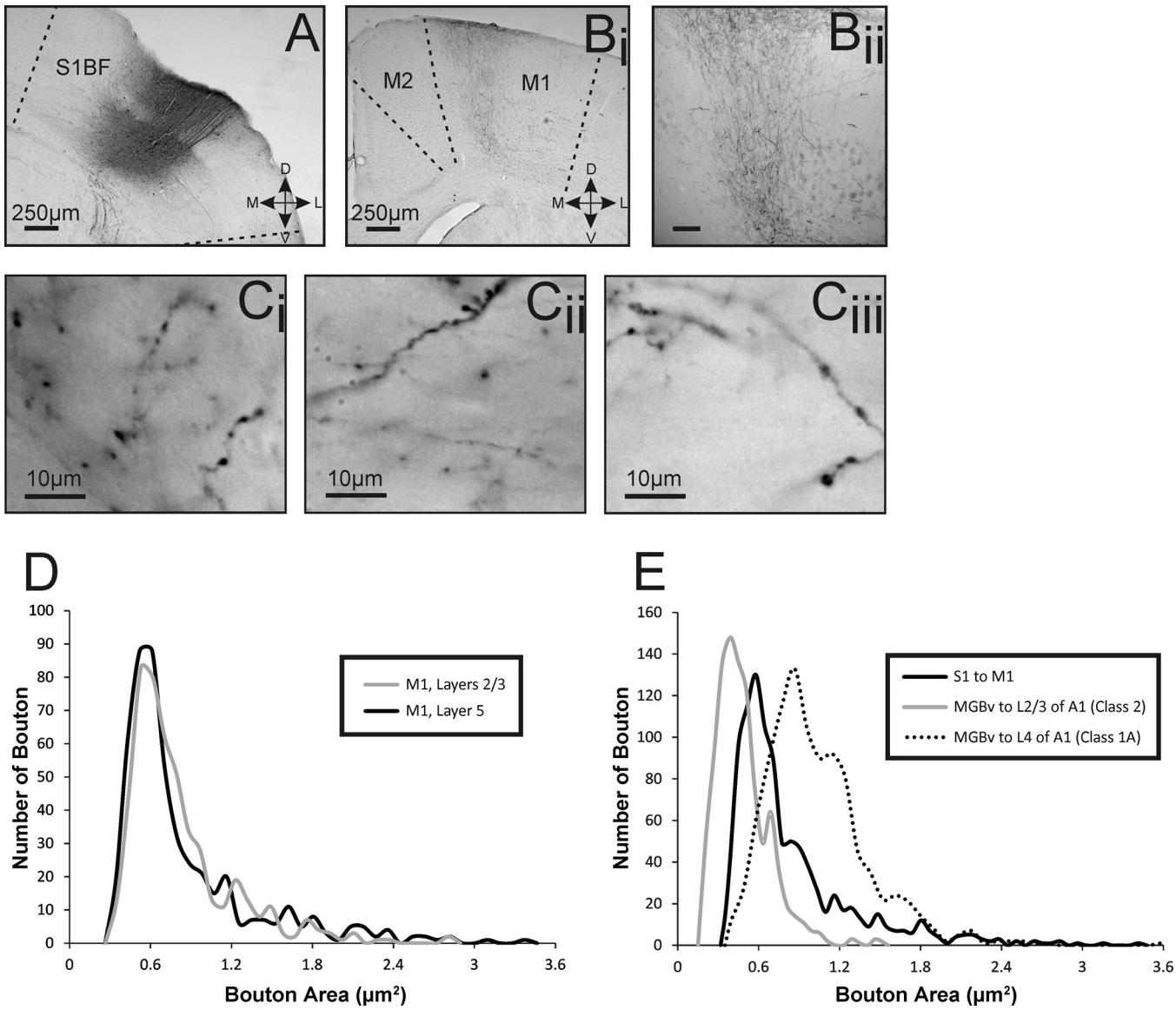

Fig. 4. Anterograde tracing in M1 after biotinylated dextran amine (BDA) injections in S1. *A*: injection site in S1 at ×5. *B*: labeling in M1 at ×5 (*Bi*) and ×10 (*Bii*). *C*: boutons in upper (*Ci* and *Cii*) and lower (*Ciii*) layers of M1, at ×100, showing variation in bouton size from small to large. *D*: histogram of bouton area in the upper and lower layers of M1. *E*: histogram of bouton area in M1 (from all layers) compared with bouton areas of a typical Class 1A and a typical Class 2 pathway (from Viaene et al. 2011b). M2, secondary motor cortex; S1BF, barrel field of S1; MGBv, ventral division of the medial geniculate body; A1, primary auditory cortex.

tinguishes Class 1B inputs (like the one we describe here) from Class 1A inputs, where such convergence does not exist or is minimal (Class 1A inputs produce responses that are "all or none"; Petrof and Sherman 2009; Reichova and Sherman 2004; Viaene et al. 2011c). All intracortical inputs described to date (both Class 1 and Class 2) exhibit a considerable degree of convergence (Covic and Sherman 2011; DePasquale and Sherman 2011, 2012).

The relatively large initial EPSPs and paired-pulse depression that we observed in the S1 input to M1 suggest that this pathway involves synapses with a high probability of glutamate release (Dobrunz and Stevens 1997), which results in gradual presynaptic depletion of the neurotransmitter and thus synaptic depression. The fact that we performed our recordings at room temperature may have increased response latencies and decreased response amplitudes in all cells, but it is unlikely to have affected the synaptic profile (depression vs. facilitation) of their responses. Furthermore, the inability to activate metabotropic glutamate receptors suggests that S1 input exerts fast and transient postsynaptic effects in M1 cells, mediated through ionotropic glutamate receptors only. These (prototypical of Class 1 inputs) features are ideal for the fast and reliable transmission of information.

In addition to their signature synaptic profile, Class 1 pathways have been associated with certain anatomical features, including the presence of a population of large terminal boutons (for a review see Petrof and Sherman 2013). Unlike Class 2 pathways, which terminate only in small boutons, Class 1 pathways terminate in boutons the size of which varies from very small ($<0.5\ \mu m^2$) to relatively large ($>1.5\ \mu m^2$). The terminal boutons of S1 inputs to M1, even though on average smaller than those of other Class 1 inputs in cortex and

thalamus (see Covic and Sherman 2011; Van Horn and Sherman 2004; Viaene et al. 2011a, 2011b), varied considerably in size and included boutons larger than 1.5 μm^2, which are rarely found in Class 2 inputs.

Previous studies (Aronoff et al. 2010; Hooks et al. 2013; Izraeli and Porter 1995; Mao et al. 2011) have reported that input to M1 arises from nearly all layers of S1, albeit with the majority originating in the subgranular layers. In our case, the observation that nearly all S1 input to M1 originated in layer 5 is most likely the result of the cutting angle used for the preparation of our slice, an angle that might have interrupted projections from other layers. Nonetheless, the observation that even after optogenetic stimulation of S1 terminals in M1 (which could activate inputs from all M1-projecting layers in S1) all responses resembled those observed from stimulation of layer 5 in S1 is indicative that the S1-to-M1 pathway may be surprisingly homogeneous.

The overall synaptic homogeneity of the S1-to-M1 pathway we report here is uncharacteristic of interareal corticocortical pathways. The reciprocal projections between primary and secondary auditory cortices are made up of both Class 1 and Class 2 inputs (Covic and Sherman 2011), and a similar mixed pattern of input classes has been seen in the reciprocal projections between the primary and secondary visual cortices (DePasquale and Sherman 2011). It is worth mentioning that, while all the responses we recorded in M1 were Class 1, we did note some layer-specific differences. Whereas the majority of cells we recorded in layers 2/3 and 5 of M1 received inputs from S1, only a minority of recorded cells did so in layer 6. This could be an artifact of the particular sectioning angle of the slice preparation we used. However, the scarcity of terminal boutons seen in layer 6 of M1 after BDA injections in S1 suggests that it is more likely that layer 6 simply receives a relatively small projection from S1. Related to this, although we did not make a distinction between layers 5A and 5B, most responsive cells (and terminal boutons) in layer 5 of M1 were located near the upper half of the layer, while lower layer 5 contained few responsive cells and labeled terminal boutons. Given that layer 5B and layer 6 contain most corticofugal M1 cells (Hooks et al. 2011), it is possible that S1 inputs avoid targeting directly the corticothalamic output cells of M1 (Mao et al. 2011). Instead, S1 inputs appear to target primarily layers 2/3 and upper layer 5, which are the same layers that project back to S1 (Petreanu et al. 2009).

S1 inputs to layer 5 of M1 are of particular interest as they evoked larger EPSPs, exhibited more synaptic depression, and were faster than those innervating layers 2/3. The functional importance of this is unclear, but it may be a significant aspect of the mechanisms controlling the internal functional circuitry of M1, for which relatively little is known. We know that the output layers of M1 are somewhat isolated from the rest of M1, since neither layers 2/3 nor upper layer 5 significantly innervates lower layer 5 and layer 6 of M1 (Hooks et al. 2011). Furthermore, since lower layer 5 and layer 6 of M1 receive little direct input from S1 (see above; also Hooks et al. 2013; Kaneko et al. 1994, 2000), despite the strong, driverlike input of S1 to other layers it is unclear how, if at all, this input affects M1 corticofugal output. Output layers of M1 receive strong inputs from the secondary motor and orbital cortices (Hooks et al. 2013), but the synaptic nature of these inputs has not been characterized thoroughly.

Conclusions. It has long been hypothesized that the output of motor cortex is heavily influenced by sensory inputs originating in both thalamus and cortex. Our data suggest that S1 in the mouse provides input capable of driving cells in the upper layers of M1. The lower layers of M1, on the other hand, receive much less input from S1, even though this quantitatively small input appears to be qualitatively similar to the one that arrives in the upper layers of M1. While a lot more needs to be understood about the internal organization of M1 before we can fully appreciate the functional contribution of these inputs, it is evident that the S1 input to motor cortical areas represents an important aspect of sensorimotor integration.

GRANTS

This work was supported by National Institute on Deafness and Other Communication Disorders Grant DC-008794 and National Eye Institute Grant EY-022338 (to S. M. Sherman) and National Institute of General Medical Sciences Medical Scientist National Research Service Award 5 T32 GM-07281 (to A. N. Viaene).

DISCLOSURES

No conflicts of interest, financial or otherwise, are declared by the author(s).

AUTHOR CONTRIBUTIONS

Author contributions: I.P., A.N.V., and S.M.S. conception and design of research; I.P. and A.N.V. performed experiments; I.P., A.N.V., and S.M.S. analyzed data; I.P., A.N.V., and S.M.S. interpreted results of experiments; I.P., A.N.V., and S.M.S. prepared figures; I.P., A.N.V., and S.M.S. drafted manuscript; I.P., A.N.V., and S.M.S. edited and revised manuscript; I.P., A.N.V., and S.M.S. approved final version of manuscript.

REFERENCES

Aronoff R, Matyas F, Mateo C, Ciron C, Schneider B, Petersen CC. Long-range connectivity of mouse primary somatosensory barrel cortex. *Eur J Neurosci* 31: 2221–2233, 2010.

Asanuma H, Hunsperger RW. Functional significance of projection from the cerebellar nuclei to the motor cortex in the cat. *Brain Res* 98: 73–92, 1975.

Brochier T, Boudreau MJ, Pare M, Smith AM. The effects of muscimol inactivation of small regions of motor and somatosensory cortex on independent finger movements and force control in the precision grip. *Exp Brain Res* 128: 31–40, 1999.

Cicirata F, Angaut P, Cioni M, Serapide MF, Papale A. Functional organization of thalamic projections to the motor cortex. An anatomical and electrophysiological study in the rat. *Neuroscience* 19: 81–99, 1986.

Covic EN, Sherman SM. Synaptic properties of connections between the primary and secondary auditory cortices in mice. *Cereb Cortex* 21: 2425–2441, 2011.

DePasquale R, Sherman SM. Synaptic properties of corticocortical connections between the primary and secondary visual cortical areas in the mouse. *J Neurosci* 31: 16494–16506, 2011.

DePasquale R, Sherman SM. Modulatory effects of metabotropic glutamate receptors on local cortical circuits. *J Neurosci* 32: 7364–7372, 2012.

DePasquale R, Sherman SM. A modulatory effect of the feedback from higher visual areas to V1 in the mouse. *J Neurophysiol* 109: 2618–2631, 2013.

Dobrunz LE, Stevens CF. Heterogeneity of release probability, facilitation, and depletion at central synapses. *Neuron* 18: 995–1008, 1997.

Franklin KB, Paxinos G. *Mouse Brain in Stereotaxic Coordinates*. Amsterdam: Elsevier Academic, 2008.

Garcia-Cabezas MA, Barbas H. Area 4 has layer IV in adult primates. *Eur J Neurosci* 39: 1824–1834, 2014.

Hiraba H, Yamaguchi Y, Satoh H, Ishibashi Y, Iwamura Y. Deficits of masticatory movements caused by lesions in the orofacial somatosensory cortex of the awake cat. *Somatosens Motor Res* 17: 361–372, 2000.

Hooks BM, Hires SA, Zhang YX, Huber D, Petreanu L, Svoboda K, Shepherd GM. Laminar analysis of excitatory local circuits in vibrissal motor and sensory cortical areas. *PLoS Biol* 9: e1000572, 2011.

Hooks BM, Mao T, Gutnisky DA, Yamawaki N, Svoboda K, Shepherd GM. Organization of cortical and thalamic input to pyramidal neurons in mouse motor cortex. *J Neurosci* 33: 748–760, 2013.

Horne MK, Tracey DJ. The afferents and projections of the ventroposterolateral thalamus in the monkey. *Exp Brain Res* 36: 129–141, 1979.

Izraeli R, Porter LL. Vibrissal motor cortex in the rat: connections with the barrel field. *Exp Brain Res* 104: 41–54, 1995.

Kaneko T, Caria MA, Asanuma H. Information processing within the motor cortex. II. Intracortical connections between neurons receiving somatosensory cortical input and motor output neurons of the cortex. *J Comp Neurol* 345: 172–184, 1994.

Kaneko T, Cho R, Li Y, Nomura S, Mizuno N. Predominant information transfer from layer III pyramidal neurons to corticospinal neurons. *J Comp Neurol* 423: 52–65, 2000.

Lam YW, Sherman SM. Activation of both Group I and Group II metabotropic glutamatergic receptors suppress retinogeniculate transmission. *Neuroscience* 242: 78–84, 2013.

Lee CC, Sherman SM. Modulator property of the intrinsic cortical projection from layer 6 to layer 4. *Front Syst Neurosci* 3: 1–5, 2009.

Li J, Guido W, Bickford ME. Two distinct types of corticothalamic EPSPs and their contribution to short-term synaptic plasticity. *J Neurophysiol* 90: 3429–3440, 2003.

Lin LD, Murray GM, Sessle BJ. The effect of bilateral cold block of the primate face primary somatosensory cortex on the performance of trained tongue-protrusion task and biting tasks. *J Neurophysiol* 70: 985–996, 1993.

Liu T, Petrof I, Sherman SM. Modulatory effects of activation of metabotropic glutamate receptors on GABAergic circuits in the mouse cortex. *J Neurophysiol* 111: 2287–2297, 2014.

Mao T, Kusefoglu D, Hooks BM, Huber D, Petreanu L, Svoboda K. Long-range neuronal circuits underlying the interaction between sensory and motor cortex. *Neuron* 72: 111–123, 2011.

Muakkassa KF, Strick PL. Frontal lobe inputs to primate motor cortex: evidence for four somatotopically organized "premotor" areas. *Brain Res* 177: 176–182, 1979.

Pavlides C, Miyashita E, Asanuma H. Projection from the sensory to the motor cortex is important in learning motor skills in the monkey. *J Neurophysiol* 70: 733–741, 1993.

Petreanu L, Mao T, Sternson SM, Svoboda K. The subcellular organization of neocortical excitatory connections. *Nature* 457: 1142–1145, 2009.

Petrof I, Sherman SM. Synaptic properties of the mammillary and cortical afferents to the anterodorsal thalamic nucleus in the mouse. *J Neurosci* 29: 7815–7819, 2009.

Petrof I, Sherman SM. Functional significance of synaptic terminal size in glutamatergic sensory pathways in thalamus and cortex. *J Physiol* 591: 3125–3131, 2013.

Porter LL, White EL. Afferent and efferent pathways of the vibrissal region of primary motor cortex in the mouse. *J Comp Neurol* 214: 279–289, 1983.

Reep RL, Goodwin GS, Corwin JV. Topographic organization in the corticocortical connections of medial agranular cortex in rats. *J Comp Neurol* 294: 262–280, 1990.

Reichova I, Sherman SM. Somatosensory corticothalamic projections: distinguishing drivers from modulators. *J Neurophysiol* 92: 2185–2197, 2004.

Rocco MM, Brumberg JC. The sensorimotor slice. *J Neurosci Methods* 162: 139–147, 2007.

Rocco-Donovan M, Ramos RL, Giraldo S, Brumberg JC. Characteristics of synaptic connections between rodent primary somatosensory and motor cortices. *Somatosens Motor Res* 28: 63–72, 2011.

Rowell JJ, Mallik AK, Dugas-Ford J, Ragsdale CW. Molecular analysis of neocortical layer structure in the ferret. *J Comp Neurol* 518: 3272–3289, 2010.

Sherman SM. Thalamocortical interactions. *Curr Opin Neurobiol* 17: 417–422, 2012.

Sherman SM, Guillery RW. *Thalamocortical Processing: Understanding the Messages that Link the Cortex to the World*. Cambridge, MA: MIT Press, 2013.

Skoglund TS, Pascher R, Berthold CH. The existence of a layer IV in the rat motor cortex. *Cereb Cortex* 7: 178–180, 1997.

Tye KM, Prakash R, Kim SY, Fenno LE, Grosenick L, Zarabi H, Thompson KR, Gradinaru V, Ramakrishnan C, Deisseroth K. Amygdala circuitry mediating reversible and bidirectional control of anxiety. *Nature* 471: 358–362, 2011.

Van Horn SC, Sherman SM. Differences in projection patterns between large and small corticothalamic terminals. *J Comp Neurol* 475: 406–415, 2004.

Viaene AN, Petrof I, Sherman SM. Properties of the thalamic projection from the posterior medial nucleus to primary and secondary somatosensory cortices in the mouse. *Proc Natl Acad Sci USA* 108: 18156–18161, 2011a.

Viaene AN, Petrof I, Sherman SM. Synaptic properties of thalamic input to layers 2/3 in primary somatosensory and auditory cortices. *J Neurophysiol* 105: 279–292, 2011b.

Viaene AN, Petrof I, Sherman SM. Synaptic properties of thalamic input to the subgranular layers of primary somatosensory and auditory cortices in the mouse. *J Neurosci* 31: 12738–12747, 2011c.

Yamawaki N, Borges K, Suter BA, Harris KD, Shepherd GM. A genuine layer 4 in motor cortex with prototypical synaptic circuit connectivity. *Elife* 3: e05422, 2014.